

# Crystal quality of two-dimensional gallium telluride and gallium selenide using Raman fingerprint

Cite as: AIP Advances 7, 015014 (2017); <https://doi.org/10.1063/1.4973918>

Submitted: 27 October 2016 • Accepted: 27 December 2016 • Published Online: 09 January 2017

Jannatul Susoma,  Jouko Lahtinen, Maria Kim, et al.



View Online



Export Citation



CrossMark

## ARTICLES YOU MAY BE INTERESTED IN

[Second and third harmonic generation in few-layer gallium telluride characterized by multiphoton microscopy](#)

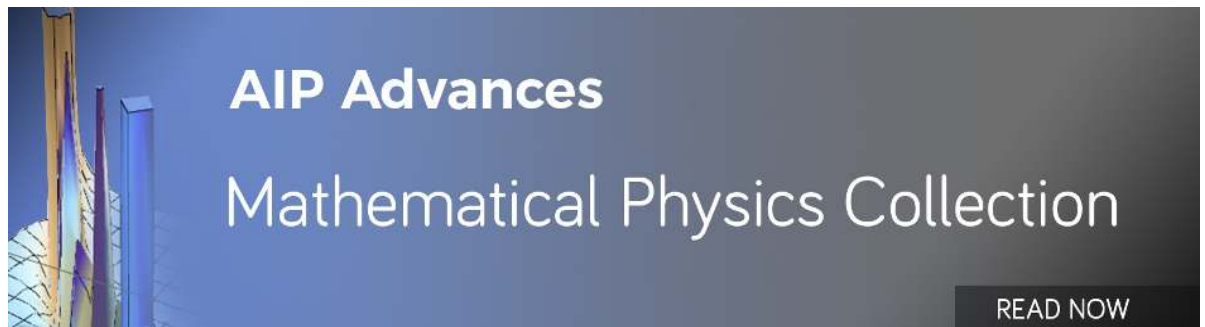
Applied Physics Letters **108**, 073103 (2016); <https://doi.org/10.1063/1.4941998>

[Oxidation of ultrathin GaSe](#)

Applied Physics Letters **107**, 173103 (2015); <https://doi.org/10.1063/1.4934592>

[Influence of thickness on crystallinity in wafer-scale GaTe nanolayers grown by molecular beam epitaxy](#)

AIP Advances **7**, 035113 (2017); <https://doi.org/10.1063/1.4978776>



AIP Advances  
Mathematical Physics Collection

READ NOW

## Crystal quality of two-dimensional gallium telluride and gallium selenide using Raman fingerprint

Jannatul Susoma,<sup>1,a</sup> Jouko Lahtinen,<sup>2</sup> Maria Kim,<sup>1</sup> Juha Riikonen,<sup>1</sup>  
and Harri Lipsanen<sup>1</sup>

<sup>1</sup>Department of Micro and Nanosciences, Aalto University, P.O. Box 13500 Aalto,  
FI-00076 Espoo, Finland

<sup>2</sup>Department of Applied Physics, Aalto University, P.O. Box 15100 Aalto, FI-00076 Espoo,  
Finland

(Received 27 October 2016; accepted 27 December 2016; published online 9 January 2017)

We have established Raman fingerprint of GaTe and GaSe to investigate their crystal quality. As unencapsulated, they both oxidise in ambient conditions which can be detected in their Raman analysis. X-ray photoelectron spectroscopy (XPS) analysis shows a good agreement with Raman analysis. 50-nm-thick Al<sub>2</sub>O<sub>3</sub> encapsulation layer deposited by atomic layer deposition (ALD) inhibits degradation in ambient conditions. © 2017 Author(s). All article content, except where otherwise noted, is licensed under a Creative Commons Attribution (CC BY) license (<http://creativecommons.org/licenses/by/4.0/>). [<http://dx.doi.org/10.1063/1.4973918>]

2D materials including insulating h-BN, semi-metallic graphene and other semiconducting layered metal chalcogenides are expected to provide new types of applications, for example to next-generation nanoelectronics and optoelectronics. GaTe and GaSe belong to the III-VI group of layered metal chalcogenides. Layered crystal structure of GaTe (GaSe) is formed by Te-Ga-Ga-Te<sup>1</sup> (Se-Ga-Ga-Se)<sup>2,3</sup> tetra-layers (TLs). Since the thickness of single-layer GaTe (GaSe) is known to be  $\sim 0.75$  nm<sup>1</sup> ( $\sim 0.98$  nm<sup>4,5</sup>), the flake thickness in nm corresponds roughly to the number of layers. Two adjacent TLs are weakly coupled via van der Waals forces.

Up to date, among the layered metal chalcogenides, MoS<sub>2</sub> is probably the most widely investigated material for device applications due to its direct bandgap in monolayer film.<sup>6,7</sup> Clear advantage compared to MoS<sub>2</sub> is that both GaTe and GaSe have a direct bandgap in the visible range (1.65 eV<sup>8-10</sup> and 1.99 eV<sup>11,12</sup>), regardless of the thickness. The direct bandgap is certainly vital for optoelectronics. Few-layer GaTe shows high prospect for transistor, photo and radiation detection applications<sup>1,13-16</sup> for example, transistor fabricated from few-layer GaTe shows exceptionally high photoresponsivity above 10<sup>4</sup> A/W,<sup>15</sup> which is significantly few tens of order higher than that of graphene (0.13 A/W<sup>17</sup>), pristine monolayer graphene (8.61 A/W<sup>18</sup>) or monolayer MoS<sub>2</sub> (880 A/W<sup>19</sup>). Single- and few-layer GaSe in transistor and photodetector applications has already been reported.<sup>2,4,5,20,21</sup> Monolayer MoS<sub>2</sub> has also gathered significant interest in recent years in nonlinear optics, as the lack of inversion symmetry yields non-vanishing second-order susceptibility.<sup>22,23</sup> In order to have second harmonic generation (SHG), it is essential to have material with broken inversion symmetry. Both GaTe and GaSe exhibit such broken inversion symmetry regardless of the number of layers,  $N$ . This is an exceptional characteristic compared to MoS<sub>2</sub>, where SHG can only be observed in case of monolayer and odd  $N$  as the inversion symmetry is broken only in these cases.<sup>22</sup> Even with odd  $N$ , the SHG signal of MoS<sub>2</sub> is significantly reduced with increasing  $N$ .<sup>22</sup> The broken inversion symmetry that persists in GaTe and GaSe regardless of  $N$  inspires to the study of those few-layer samples. Both GaTe and GaSe are non-centrosymmetric 2D layered materials, where GaTe has a monoclinic crystal structure, and in case of GaSe, it is hexagonal. The top and side views of the hexagonal GaSe structure are presented in Figure 1(a) and Figure 1(b), and the monoclinic GaTe are presented in

<sup>a</sup>Electronic mail: [jannatul.susoma@aalto.fi](mailto:jannatul.susoma@aalto.fi)

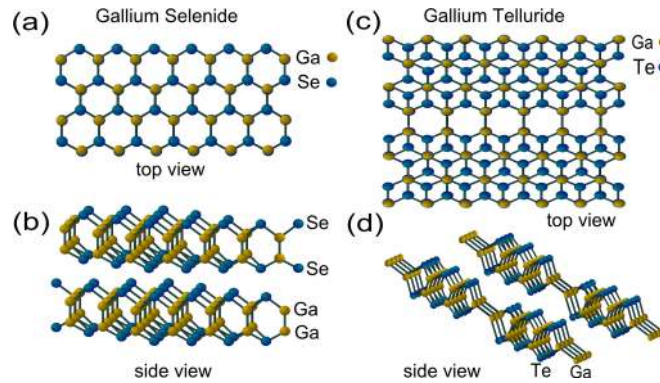


FIG. 1. The top and side views of the hexagonal GaSe (a), (b) and monoclinic GaTe (c), (d) structural models.

Figure 1(c) and Figure 1(d). Strong second-harmonic generation (SHG) and third-harmonic generation (THG) have already been reported for few-layer GaTe<sup>24</sup> and GaSe.<sup>25</sup> Crystal non-centrosymmetry is essential for SHG. As 2D materials, they provide additional advantages over bulk, such as atomically thin layers provide a pathway towards novel responses arising from 2D heterostructures, for example graphene-GaSe.<sup>26</sup> However, the surface of GaTe and GaSe oxidize over time in ambient condition. Recent reports have shown atmospheric induced degradation of optical properties of ultrathin GaSe.<sup>27</sup> Thermally activated Ga vacancy defects in multilayer GaTe has been reported in field effect transistor (FET) and phototransistor application.<sup>28</sup> The thicknesses dependent PL of GaTe and GaSe films has also been reported, where in both materials, PL shows a dramatic decrease of intensity at a reduced film thickness due to non-radiative carrier escape via surface states. Thus, the need for surface passivation of the GaTe and GaSe films has also been emphasized.<sup>29</sup> Investigation of the crystal quality of 2D GaTe and GaSe using Raman fingerprint has not yet been studied intensively.

In this study, we present a systematic Raman analysis to monitor the quality of GaTe and GaSe due to oxidation in ambient condition. The time dependent atmospheric degradation of these materials is examined separately for both materials. We also carried out XPS analysis to understand the oxidation effect of GaTe and GaSe surfaces. Systematic stability study as a function of time was carried out focusing on Raman fingerprint of few-layer GaTe and GaSe to identify their crystal quality, which is vital to understand the oxidation process of the materials in ambient condition. It is also highly beneficial to have a straightforward method to evaluate material quality. The Raman fingerprint established in this study is therefore highly beneficial in this regard. We confirm that the 50 nm ALD protects flakes from ambient oxidation, which can also be beneficial for device applications and material integration point of view.

Raman active lattice vibrational modes of GaTe and GaSe have been investigated at room temperature in the range from 50  $\text{cm}^{-1}$  to 350  $\text{cm}^{-1}$ . We have recorded Raman spectra as a function of time from freshly cleaved to several weeks old flakes stored in the ambient air. For each sample, Raman and photoluminescence (PL) spectra were simultaneously recorded by LabRAM confocal micro Raman system utilizing  $\sim 6$  mW of 514 nm and  $\sim 3$  mW of 633 nm lasers coupled to 100 $\times$ /0.95 NA air objective resulting in a spot size of  $\sim 1$   $\mu\text{m}$ . Measurements were carried out in ambient air at room temperature. Figure 2 presents Raman spectra of GaTe and GaSe exhibiting the characteristic responses of both of the materials. PL displays a maximum near 1.65 eV and 2 eV, which is consistent with the bandgap of GaTe and GaSe, respectively.

About ten distinct Raman modes in the spectrum at 52  $\text{cm}^{-1}$ , 66  $\text{cm}^{-1}$ , 76  $\text{cm}^{-1}$ , 109  $\text{cm}^{-1}$ , 115  $\text{cm}^{-1}$ , 162  $\text{cm}^{-1}$ , 175  $\text{cm}^{-1}$ , 207  $\text{cm}^{-1}$ , 268  $\text{cm}^{-1}$ , and 282  $\text{cm}^{-1}$  are observed from freshly cleaved GaTe as shown in Figure 2(a) and match the reported data very well with the bulk GaTe.<sup>30</sup> The peaks at 123  $\text{cm}^{-1}$  and 140  $\text{cm}^{-1}$  due to ambient oxidation can be observed within few hours of exfoliation of GaTe, which are slightly noticeable or nearly undetectable in freshly cleaved GaTe. Due to oxidation, the GaTe Raman peak and the PL intensities decrease whereas the new peaks at wavenumber 123  $\text{cm}^{-1}$  and 140  $\text{cm}^{-1}$  become prominent over time. Figure 2(b) and Figure 2(c) show Raman and PL spectra,

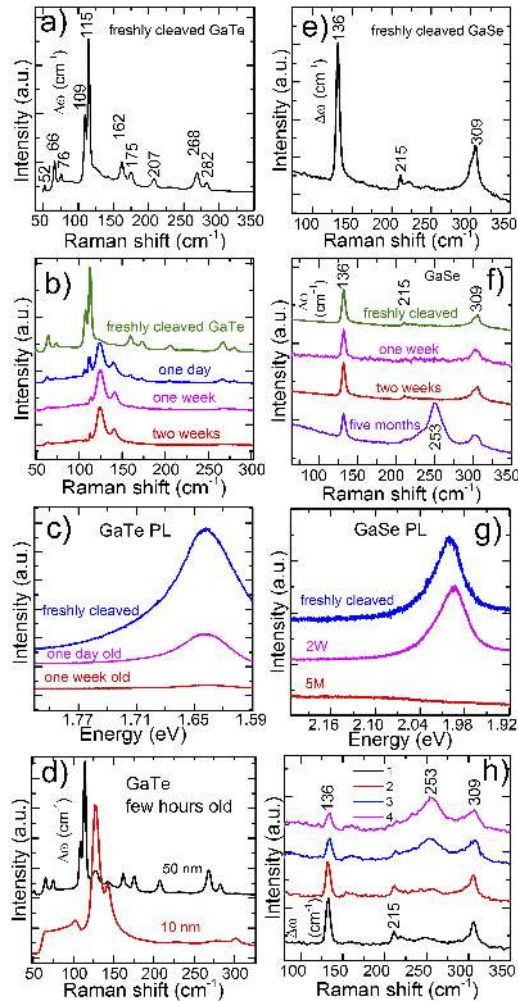


FIG. 2. Raman spectra of freshly cleaved GaTe (a) and GaSe (e) are presented. Raman shift is symbolized as  $\Delta\omega$ . Raman spectrum and photoluminescence (PL) of freshly cleaved GaTe (b-c) and GaSe (f-g) are plotted as a function of oxidation time. (d) Peaks at  $123\text{ cm}^{-1}$  and  $140\text{ cm}^{-1}$  due to ambient oxidation are more prominent in thin (10 nm) GaTe even in few hours of air exposure, whereas in the case of thin GaSe flake, the oxidised peak is non-detectable in Raman even after few weeks of air exposure. (h) Laser enhanced oxidation was carried out to oxidise GaSe intentionally because unlike GaTe, GaSe shows slower oxidation in ambient condition. The number of laser exposures is from 1 to 4.

respectively, as a function of oxidation time in ambient air. Eventually, entirely oxidised GaTe shows only two Raman peaks at  $123\text{ cm}^{-1}$  and  $140\text{ cm}^{-1}$ , while other peaks disappear. Thin flakes oxidise entirely compared to the thicker ones within the same time frame as shown in Figure 2(d). It should be noted that the two peaks at  $123\text{ cm}^{-1}$  and  $140\text{ cm}^{-1}$  match the reported data for the few-layer,<sup>30</sup> multilayer<sup>15</sup> and also bulk GaTe,<sup>15</sup> where the flakes possibly oxidised already during the exfoliation process.

Freshly cleaved GaSe shows four prominent peaks at  $136\text{ cm}^{-1}$ ,  $215\text{ cm}^{-1}$ ,  $233\text{ cm}^{-1}$ , and  $309\text{ cm}^{-1}$  as shown in Figure 2(e). Due to oxidation, amorphous selenium (a-Se) is formed at the surface which exhibits a broad Raman peak near  $253\text{ cm}^{-1}$  with a shoulder at  $234\text{ cm}^{-1}$ . This result shows a good agreement with the recent report.<sup>27</sup> Oxidation also produces  $\text{Ga}_2\text{Se}_3$  and  $\text{Ga}_2\text{O}_3$  which can be detected by Raman at  $150\text{ cm}^{-1}$  and at  $233\text{ cm}^{-1}$ , respectively.<sup>27</sup> These two peaks at  $150\text{ cm}^{-1}$  and at  $233\text{ cm}^{-1}$  are not clearly visible in our Raman measurements. The a-Se peak becomes prominent due to oxidation whereas intensities of other GaSe peaks reduce. Figure 2(f) shows that the Raman mode at  $253\text{ cm}^{-1}$  is undetectable within two weeks of ambient condition, whereas within five months the peak at  $253\text{ cm}^{-1}$  becomes quite prominent. Thin flakes oxidise entirely compared

to the thicker ones over a certain period of time. Unlike GaTe, ambient oxidation is rather slow in GaSe. In order to enhance the oxidation process, laser was used to oxidise GaSe intentionally. The change of Raman modes due to laser assisted oxidation is shown in Figure 2(h), where the intensity ratio of the mode at  $253\text{ cm}^{-1}$  to that at  $136\text{ cm}^{-1}$  increase with the number of laser exposure (1 to 4). This reveals that the peaks developed at  $253\text{ cm}^{-1}$  and  $234\text{ cm}^{-1}$  are due to the oxidation of GaSe. No PL is detected from GaTe (thickness 220 nm) after one week of ambient oxidation, as plotted in Figure 2(c). On the other hand, the PL remains quite intense in GaSe (thickness 50 nm) even after two weeks of ambient oxidation although it disappears in five months, as can be seen in Figure 2(g). Oxidation produces layers of both metal and tellurium oxides on the GaTe surface.<sup>31</sup> Metallic Te shows Raman peaks at  $123\text{ cm}^{-1}$  and  $140\text{ cm}^{-1}$ , which is in agreement with previous report (peaks at  $122\text{ cm}^{-1}$  and  $141\text{ cm}^{-1}$ <sup>32</sup>). Raman peaks at  $122\text{ cm}^{-1}$ ,  $149\text{ cm}^{-1}$ ,  $174\text{ cm}^{-1}$ , and  $196\text{ cm}^{-1}$  originating from  $\text{TeO}_2$  have also been reported<sup>32</sup> which is not that prominent in our case.

Freshly cleaved GaTe and GaSe showing atomically smooth surface are presented in Figure 3(a) and Figure 3(d), respectively. Roughness ( $R_a$ ) increases from 0.14 to 1.70 nm in a year due to the ambient oxidation of GaSe (thickness 12 nm) as shown in Figure 3(e). However, the one-year-old GaTe shows a surface as smooth as the freshly cleaved samples. The freshly cleaved GaTe (thickness 220 nm) has a roughness of 0.08 nm and the roughness remains unchanged over the year exposed in ambient condition shown in Figure 3(b). Figure 3(c) shows AFM cross-sections taken from the blue dashed line A-A' in image (a) and green dashed line B-B' in image (b) showing their roughness from freshly cleaved and a year old GaTe. Figure 3(f) shows AFM cross-sections taken from the blue dashed line A-A' in image (d) and green dashed line B-B' in image (e) showing their roughness from freshly cleaved and a year old GaSe. Change of roughness is higher in GaSe than in GaTe after air exposure in the same time frame.

A 50-nm-thick  $\text{Al}_2\text{O}_3$  layer was deposited by ALD on mechanically exfoliated GaTe and GaSe, where they show no evidence of ambient oxidation even after six weeks of air exposure. Raman spectra and PL as a function of time (one day to six weeks) of ALD encapsulated GaTe are shown in Figure 4(a) and Figure 4(b), respectively. Similarity, Figure 4(c) and Figure 4(d) present results from

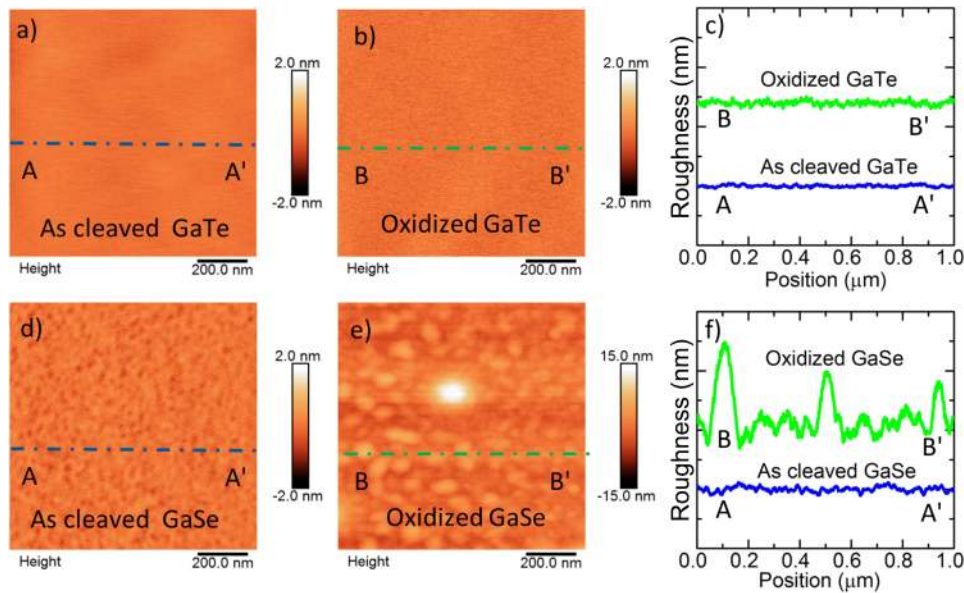


FIG. 3. Surface roughness of GaTe and GaSe as a function of time. AFM images and their cross-sections used to determine their surface roughness from freshly cleaved and a year old GaTe and GaSe. (a) Freshly cleaved and (b) a year old of GaTe flake. (c) AFM cross-sections taken from the blue dashed line A-A' in image (a) and green dashed line B-B' in image (b) showing their roughness from freshly cleaved and a year old GaTe. (d) Freshly cleaved and (e) a year old of GaSe flake. (f) AFM cross-sections taken from the blue dashed line A-A' in image (d) and green dashed line B-B' in image (e) showing their roughness from freshly cleaved and a year old GaSe.



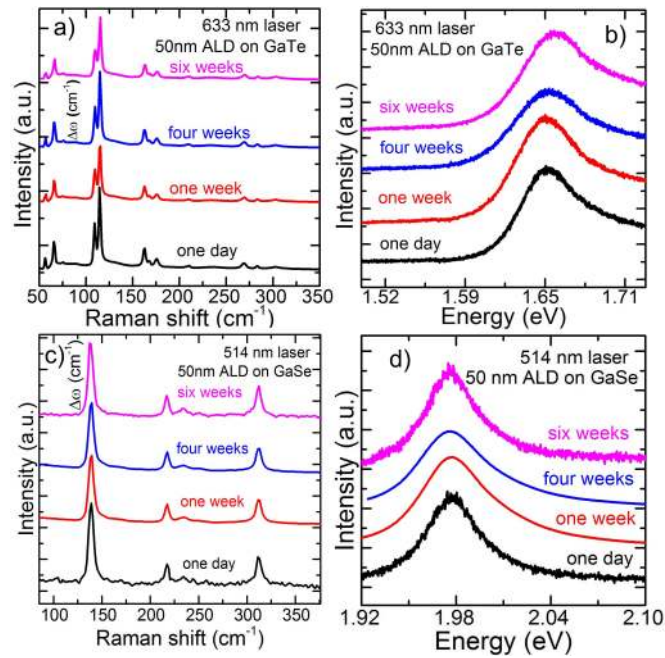


FIG. 4. Raman spectra of GaTe and GaSe encapsulated by 50 nm ALD  $\text{Al}_2\text{O}_3$  as function of time. Raman spectra and PL of ALD encapsulated GaTe (a and b, respectively) and GaSe (c and d, respectively) in different times (one day to six weeks).

GaSe. The peak at  $233\text{ cm}^{-1}$ , which may have generated from partly oxidised GaSe (i.e.  $\text{Ga}_2\text{O}_3$ ) is not that prominent in our Raman spectrum. The ALD encapsulated samples do not oxidise in ambient air within six weeks of observation.

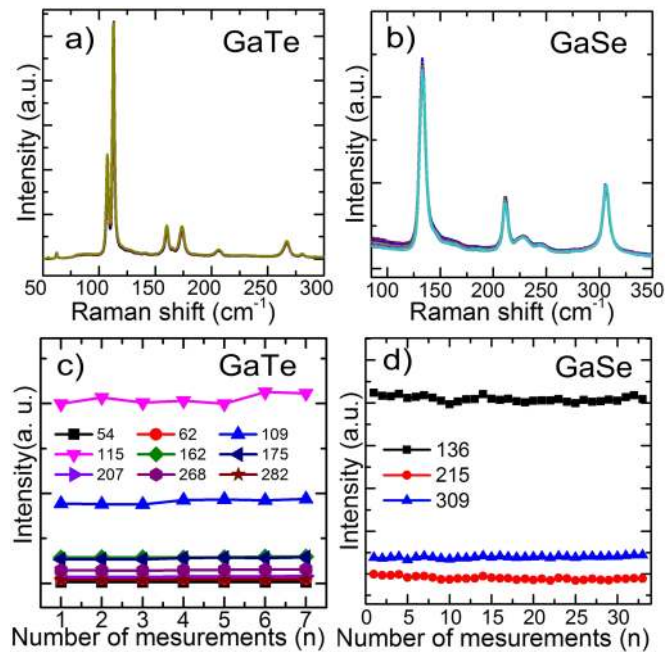


FIG. 5. 50 nm ALD on GaTe and GaSe as a function of laser assisted annealing. Oxidised peaks are practically undetectable from both GaTe (a) and GaSe (b). The peak intensities were almost invariant even with several laser exposures in both materials (c) and (d).

Figure 5(a) and Figure 5(b) show Raman spectrum from 50 nm ALD encapsulated GaTe and GaSe, respectively, as a function of laser assisted annealing. 50 nm ALD  $\text{Al}_2\text{O}_3$  passivated surface shows no change in Raman peaks, hence no evidence of material degradation. Raman spectrum remains the same as the freshly cleaved ones even after several Raman spectra were taken from the same position, which reveals that there is no laser assisted oxidation with 50 nm ALD encapsulated flakes, whereas without ALD laser assisted annealing results in significant degradation. Figure 5(c) and Figure 5(d) show the invariant Raman peaks for both materials with several measurements.

Binding energy of Ga  $2p_{3/2}$  of freshly cleaved GaSe is 1117.5 eV.<sup>33</sup> Binding energy of Ga  $2p_{3/2}$  of freshly cleaved GaSe increases from 1117.5 eV to 1118.1 eV within one month of exposure in air, and it remains at the same position for three months of air exposure, as observed in Figure 6(a). This upward shift can be interpreted as partial oxidation of the surface. Reference values for gallium oxide vary from 1117.5 to 1119.0 eV.<sup>34</sup> Figure 6(b) shows, in the freshly cleaved GaSe, the Se 3d peak is observed at 54.7 eV, which can originate either from elemental Se<sup>34</sup> or GaSe.<sup>35</sup> After one month in air the Se 3d peak remains at the original position but after three months in air the peak shifts to 59.2 eV, which is a typical value for an oxide.

Figure 6(c) compares the Ga  $2p_{3/2}$  XPS spectra of (1) a freshly cleaved surface of GaTe, (2) the same surface exposed to atmosphere for a month, and (3) for three months. In the freshly cleaved GaTe, the Ga 2p peak at 1117.8 eV which can be interpreted as GaTe.<sup>36</sup> After one month in ambient condition the Ga 2p peak shifts to 1118.3 eV, and after three months to 1118.6 eV. This upward shift can be interpreted as an oxidation of the surface. A value of 1118.4 eV for oxide has already been reported.<sup>36</sup> The Te 3d peak consists of two separate features. The peak around 573 eV represents GaTe and the other at 576 eV represents tellurium oxide.<sup>36</sup> The binding energy for elemental Te is only slightly smaller than that of GaTe.<sup>36</sup> In the freshly cleaved GaTe only a small fraction (10%) of Te is oxidised but its relative amount increases in the air; after one month it is already 30% and after three months 44%, as shown in Figure 6(d). XPS shows clear evidence of ambient oxidation of the material surfaces which is consistent with the established Raman fingerprint of this study.

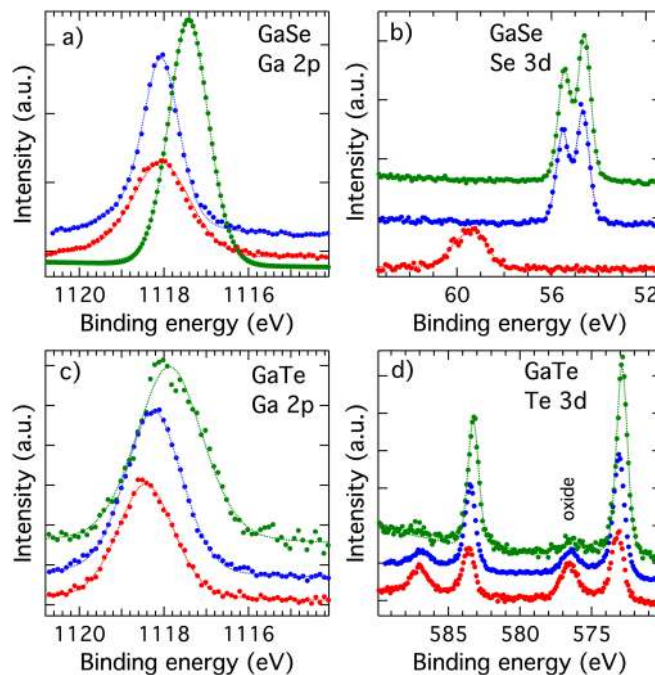


FIG. 6. XPS spectra of both GaSe and GaTe. Energy shifts to higher energy upon atmospheric exposure indicates oxidation in both materials. XPS spectra of binding energy of Ga 3p of GaSe (a) and GaTe (c) during ambient oxidation includes freshly cleaved (green), one month (blue) and three months (red) old samples. Spectrum of binding energy of Se 3d of GaSe (b) and Te 3d of GaTe (d) during ambient oxidation (freshly cleaved, one month and three months old).

We have established a Raman fingerprint of GaTe and GaSe to evaluate their crystalline quality especially in relation to material oxidation. As many other two-dimensional materials, gallium chalcogenides such as GaTe and GaSe are unstable materials as they oxidise in ambient condition. Oxidisation is a rapid process in case of GaTe whereas GaSe is less susceptible to oxidation. XPS results confirm our Raman analysis. Our results further emphasize that the surface passivation with ALD Al<sub>2</sub>O<sub>3</sub> is beneficial to inhibit atmospheric degradation of two-dimensional gallium chalcogenides. Hereby, it is vital to understand the oxidation process as then the device fabrication process and be designed accordingly. Additionally, it is also highly beneficial to have a straight forward method to evaluate material quality. The Raman fingerprint established in this study is therefore highly useful in this regard.

**Sample preparation:** Few-layer flakes of GaTe and GaSe were obtained by mechanical cleaving from a bulk single crystal, where both of the materials were grown by the Bridgman method. Utilizing adhesive tape, exfoliation was carried out in ambient air. Flakes were deposited on an oxidised silicon substrate with an oxide thickness of 285 nm. Few-layer flakes were identified using optical microscopy, and the flake thickness and surface morphology were determined by atomic force microscopy (AFM).

**Raman spectroscopy:** A confocal scanning micro-Raman system with 514 nm green and 633 nm red lasers were used to measure samples at room temperature in ambient air utilizing ~6 mW of 514 nm and ~3 mW of 633 nm laser coupled to 100×/0.95 NA air objective resulting in a spot size of ~1 μm. The accumulation time 5s was used to acquire the Raman spectra of the time dependent measurements. Raman and photoluminescence (PL) spectra were simultaneously recorded. Initially, the measurements were carried out within a few hours after mechanical cleaving to avoid any degradation of the samples. Later, time dependent measurements were carried out in order to spot the spectral differences due to oxidisation for both the materials. The spectra were averaged from five measurements in the different regions. The oxidation spectral dependence of the Raman signal according to sample thickness was also observed. Time dependent measurements were also carried out for ALD encapsulated samples. No spectral dependence of the Raman signal on ALD encapsulated samples in the same region were observed in both cases. Controlled experimental procedures, such as avoiding exposure to high laser power, were employed to minimize possible degradation of GaTe and GaSe.

**X-ray photoelectron spectroscopy:** We used a Kratos Axis Ultra for the X-ray Photoemission Spectroscopy (XPS). The measurements were performed with monochromatic Al Kα (1486.6 eV) source. We started the measurements with XPS imaging using Ga 2p peak and selected the measurement positions based on the images to minimize the contribution from the support material. The XPS spectra were recorded with an analysis spot diameter of 55 μm and 27 μm. The pass energy was 20 eV. XPS was employed to investigate ambient oxidation of the crystals.

**Atomic layer deposition:** Atomic layer deposition is technique that can produce thin films. ALD processes vapour phase chemicals in a cyclic in self-saturating fashion. The operation of ALD is based on the sequential use of a precursor gas or vapour phase chemicals. The source vapours are pulsed into the reactor which results in a unique self-limiting film growth. The deposition continues to repeat the cyclic procedure until appropriate film thickness is achieved. 50 nm-thick Al<sub>2</sub>O<sub>3</sub> was deposited instantly on mechanically exfoliated GaTe (GaSe) to avoid atmospheric degradation. The thickness of 50 nm with a deposition temperature 300°C was chosen to have an excellent quality of ALD.

This work is financed by the Academy of Finland, TEKES - the Finnish Funding Agency for Technology and Innovation under NP-Nano project, the Graphene Flagship in European Union Seventh framework Programme under grant no. 604391 and in Horizon 2020 GrapheneCore1 under grant no. 696656. We also acknowledge the provision of technical facilities of the Micronova, Nanofabrication Centre of Aalto University and OtaNano - Nanomicroscopy Center (Aalto-NMC) of Aalto University.

<sup>1</sup> P. Hu, J. Zhang, M. Yoon, X. Qiao, X. Zhang, W. Feng, P. Tan, W. Zheng, J. Liu, X. Wang, J. C. Idrobo, D. B. Geohegan, and K. Xiao, *Nano Res.* **7**, 694 (2014).

<sup>2</sup> Y. Zhou, Y. Nie, Y. Liu, K. Yan, J. Hong, C. Jin, Y. Zhou, J. Yin, Z. Liu, and H. Peng, *ACS Nano* **8**, 1485 (2014).

<sup>3</sup> W. Jie, X. Chen, D. Li, L. Xie, Y. Y. Hui, S. P. Lau, X. Cui, and J. Hao, *Angew. Chem. Int. Ed. Engl.* **54**, 1185 (2015).

<sup>4</sup> D. J. Late, B. Liu, H. S. S. R. Matte, C. N. R. Rao, and V. P. Dravid, *Adv. Funct. Mater.* **22**, 1894 (2012).



- <sup>5</sup> P. Hu, Z. Wen, L. Wang, P. Tan, and K. Xiao, *ACS Nano* **6**, 5988 (2012).
- <sup>6</sup> K. F. Mak, C. Lee, J. Hone, J. Shan, and T. F. Heinz, *Phys. Rev. Lett.* **105**, 136805 (2010).
- <sup>7</sup> A. Splendiani, L. Sun, Y. Zhang, T. Li, J. Kim, C.-Y. Chim, G. Galli, and F. Wang, *Nano Lett.* **10**, 1271 (2010).
- <sup>8</sup> C. Tatsuyama, Y. Watanabe, C. Hamaguchi, and J. Nakai, *J. Physical. Soc. Japan.* **29**, 150 (1970).
- <sup>9</sup> S. Pal and D. N. Bose, "Growth, characterisation and electrical anisotropy in layered chalcogenides GaTe and InTe," *Solid State Commun.* **97**, 725 (1996).
- <sup>10</sup> J. F. Sánchez-Royo, J. Pellicer-Porres, A. Segura, V. Muñoz-Sanjosé, G. Tobías, P. Ordejón, E. Canadell, and Y. Huttel, *Phys. Rev. B* **65**, 115201 (2002).
- <sup>11</sup> E. Mooser and M. Schlüter, *Nuovo Cimento. C.* **18**, 164 (1973).
- <sup>12</sup> V. Capozzi and M. Montagna, *Phys. Rev. B* **40**, 3182 (1989).
- <sup>13</sup> K. C. Mandal, R. M. Krishna, T. C. Hayes, P. G. Muzykov, S. Das, T. S. Sudarshan, and S. Ma, *IEEE Trans. Nucl. Sci.* **58**, 1981 (2011).
- <sup>14</sup> Z. Wang, M. Safdar, M. Mirza, K. Xu, Q. Wang, Y. Huang, F. Wang, X. Zhan, and J. He, *Nanoscale* **7**, 7252 (2015).
- <sup>15</sup> F. Liu, H. Shimotani, H. Shang, T. Kanagasekaran, V. Zolyomi, N. Drummond, V. I. Falko, and K. Tanigaki, *ACS Nano* **8**, 752 (2014).
- <sup>16</sup> P. Reshmi, A. Kunjomana, K. Chandrasekharan, M. Meena, and C. Mahadevan, *Int. J. Soft Comput. Eng.* **1**, 228 (2011).
- <sup>17</sup> X. Wang, Z. Cheng, K. Xu, H. K. Tsang, and J.-B. Xu, *Nat. Photonics.* **7**, 888 (2013).
- <sup>18</sup> Y. Zhang, T. Liu, B. Meng, X. Li, G. Liang, X. Hu, and Q. J. Wang, *Nat. Commun.* **4**, 1811 (2013).
- <sup>19</sup> O. Lopez-Sanchez, D. Lembke, M. Kayci, A. Radenovic, and A. Kis, *Nat. Nanotechnol.* **8**, 497 (2013).
- <sup>20</sup> D. J. Late, B. Liu, J. Luo, A. Yan, H. Matte, M. Grayson, C. Rao, and V. P. Dravid, *Adv. Mater.* **24**, 3549 (2012).
- <sup>21</sup> S. Lei, L. Ge, Z. Liu, S. Najmaei, G. Shi, G. You, J. Lou, R. Vajtai, and P. M. Ajayan, *Nano Lett.* **13**, 2777 (2013).
- <sup>22</sup> Y. Li, Y. Rao, K. F. Mak, Y. You, S. Wang, C. R. Dean, and T. F. Heinz, *Nano Lett.* **13**, 3329 (2013).
- <sup>23</sup> L. M. Malard, T. V. Alencar, A. P. M. Barboza, K. Fai Mak, and A. M. de Paula, *Phys. Rev. B* **87**, 201401 (2013).
- <sup>24</sup> J. Susoma, L. Karvonen, A. Säynätjoki, S. Mehravar, R. Norwood, N. Peyghambarian, K. Kieu, H. Lipsanen, and J. Riikonen, *Appl. Phys. Lett.* **108**, 073103 (2016).
- <sup>25</sup> L. Karvonen, A. Säynätjoki, S. Mehravar, R. D. Rodriguez, S. Hartmann, D. R. T. Zahn, S. Honkanen, R. A. Norwood, N. Peyghambarian, K. Kieu, H. Lipsanen, and J. Riikonen, *Sci. Rep.* **5**, 10334 (2015).
- <sup>26</sup> W. Kim, C. Li, F. A. Chaves, D. Jiménez, R. D. Rodriguez, J. Susoma, M. A. Fenner, H. Lipsanen, and J. Riikonen, *Adv. Mater.* **28**, 1845 (2016).
- <sup>27</sup> T. E. Beechem, B. M. Kowalski, M. T. Brumbach, A. E. McDonald, C. D. Spataru, S. W. Howell, T. Ohta, J. A. Pask, and N. G. Kalugin, *Appl. Phys. Lett.* **107**, 173103 (2015).
- <sup>28</sup> Z. Wang, K. Xu, Y. Li, X. Zhan, M. Safdar, Q. Wang, F. Wang, and J. He, *ACS Nano* **8**, 4859 (2014).
- <sup>29</sup> O. D. Pozo-Zamudio, S. Schwarz, M. Sich, I. A. Akimov, M. Bayer, R. C. Schofield, E. A. Chekhovich, B. J. Robinson, N. D. Kay, O. V. Kolosov, A. I. Dmitriev, G. V. Lashkarev, D. N. Borisenko, N. N. Kolesnikov, and A. I. Tartakovskii, *2D Mater.* **2**, 035010 (2015).
- <sup>30</sup> Q. Zhao, T. Wang, Y. Miao, F. Ma, Y. Xie, X. Ma, Y. Gu, J. Li, J. He, B. Chen, S. Xi, L. Xu, H. Zhen, Z. Yin, J. Li, J. Ren, and W. Jie, *Phys. Chem. Chem. Phys.* **18**, 18719 (2016).
- <sup>31</sup> O. A. Balitskii and W. Jaegermann, *Mater. Chem. Phys.* **97**, 98 (2006).
- <sup>32</sup> W. D. Bonificio and D. R. Clarke, *J. Appl. Microbiol.* **117**, 1293 (2014).
- <sup>33</sup> O. Lang, Y. Tomm, R. Schlaf, C. Pettenkofer, and W. Jaegermann, *J. Appl. Phys.* **75**, 7814 (1994).
- <sup>34</sup> A. Naumkin, A. Kraut-Vass, S. Gaarenstroom, and C. Powell, Database 20, Version 4.1, (2012), <http://srdata.nist.gov/xps/>.
- <sup>35</sup> S. Chegwiddden, Z. Dai, M. A. Olmstead, and F. S. Ohuchi, *J. Vac. Sci. Technol. A* **16**, 2376 (1998).
- <sup>36</sup> K. C. Mandal, T. Hayes, P. G. Muzykov, R. Krishna, S. Das, T. S. Sudarshan, and S. Ma, *Proc. SPIE Int. Soc. Opt. Eng.* **7805**, 78050Q1 (2010).